International Journal of Heat and Mass Transfer 54 (2011) 345–355

Contents lists available at ScienceDirect

International Journal of Heat and Mass Transfer

journal homepage: www.elsevier.com/locate/ijhmt

A three-dimensional numerical model of thermoelectric generators in fluid power systems

Min Chen *, Lasse A. Rosendahl, Thomas Condra

Institute of Energy Technology, Aalborg University, Pontoppidanstraede 101, DK-9220 Aalborg, Denmark

ARTICLE INFO

Article history:
Received 31 May 2010
Received in revised form 13 August 2010
Accepted 19 August 2010
Available online 12 October 2010

Keywords:
Thermoelectric generator
Heat transfer
Thermal fluid
System modeling

ABSTRACT

In thermoelectric generators, the heat sources are usually fluids or flames. To simplify the co-design and co-optimization of the fluid or combustion system and the thermoelectric device, which are crucial for maximizing the system performance, a three-dimensional thermoelectric generator model is proposed and implemented in a computational fluid dynamics (CFD) simulation environment (FLUENT). This model of the thermoelectric power source accounts for all temperature dependent characteristics of the materials, and includes nonlinear fluid-thermal-electric multi-physics coupled effects. In solid regions, the heat conduction equation is solved with ohmic heating and thermoelectric source terms, and user defined scalars are used to determine the electric field produced by the Seebeck potential and electric current throughout the thermoelements. The current is solved in terms of the load value using user defined functions but not a prescribed parameter, and thus the field-circuit coupled effect is included. The model is validated by simulation data from other models and experimental data from real thermoelectric devices. Within the common CFD simulator FLUENT, the thermoelectric model can be connected to various CFD models of heat sources as a continuum domain to predict and optimize the system performance.

1. Introduction

Thermoelectric generators are unique power sources that directly convert heat into electricity by means of semiconductor materials. They are of great interest in energy applications due to their well-known merits such as high durability and environmental friendliness, and they recover thermal energy to generate power in a simple manner. Thermoelectric devices have been installed in automobile exhaust pipes to reduce the power load on the vehicle's alternator [1], and in biomass or gas fired heaters to provide power for fluorescent lights, TVs, pumps, fans or control panels [2–6]. Another kind of design has integrated thermoelectric generators in various micro-reactors and micro-combustors as miniature power sources for portable/mobile electronic devices and sensor network nodes to compete with low energy density electrochemical batteries and fuel cells with complex on-board reformers [7–15]. The concept of combustion-driven thermoelectric generation has also been implemented in sophisticated configurations of active counterflow heat exchangers and reciprocating flow combustion in porous materials [16–18].

When thermoelectric devices are coupled with these fluid and combustion systems, the interaction between the heat source and the generator is critical to the overall performance. Although the power generation and efficiency of thermoelectric generators have been discussed at length, their influence on the heat source can be important as well [1,3,9,12]. To identify the impact of incorporating thermoelectric generators into energy systems and to design a new generation of power applications with increased performance, modeling and design at the system level are mandatory. In practical applications, the majority of heat sources for thermoelectric generators are in fluid form, whereas thermoelectric effects are described by solid heat transfer terms. Thus, the main challenge in the development of such system models is to simulate the fluid-structure coupled multiphysics effects, and the temperature gradients across the top and bottom surfaces of the thermoelectric generator and across the contact surfaces of the hot and cold source fluids should depend upon each other, i.e., using the third kind of thermal boundary conditions instead of the first or second. The designer must integrate the thermoelectric device model into the fluid model, and the system optimization (combustion control and combustor design, channel and heat exchanger shape, flow rate, inlet direction, etc.) must be done in conjunction with the thermoelectric generator optimization (geometry of pellets, segmentation/cascade, and deployment of modules/thermocouples, among others).

Thus far, a number of system models have been proposed by coupling the analytical thermoelectric model with various fluid models obtained from simplified assumptions for specific applications [19–29]. These system models are useful in the rough

* Corresponding author. Tel.: +45 60902482; fax: +45 9815 1411.
E-mail address: mch@et.aau.dk (M. Chen).

0017-9310/$ - see front matter © 2010 Elsevier Ltd. All rights reserved.
doi:10.1016/j.ijheatmasstransfer.2010.08.024

Nomenclature

C	capacitance
c	specific heat of the element
I	current
J	electric current density
k	thermal conductivity of the material
K_1	interface thermal conductance between the generator and the hot fluid source
K_2	interface thermal conductance between the generator and the cold fluid source
L	length of the p- and n-type legs
m	mass density of the element
P	power on the load
q	heat flow density in the leg
Q_c	rate of heat transfer from the cold junction to the heat sink
Q_h	rate of heat transfer from the heat source to the hot junction
R	generator internal resistance
R_l	load resistance
$R_{p,n}$	resistance of the p- or n-type leg
S	uniform cross-sectional area of the leg
T	temperature distribution of the leg
t	time
T_a	temperature of the cold fluid source
T_c	temperature of the cold junction
T_h	temperature of the hot junction
T_w	temperature of the hot fluid source
V	electric potential
x,y,z	directions of the 3D coordinate system

Greek symbols

α	Seebeck coefficient of the device, $\alpha = \alpha_p - \alpha_n$
$\alpha_{p,n}$	Seebeck coefficient of the p- or n-type material
ΔT	temperature difference across the element
η	efficiency
ρ	electrical resistivity of the material

Subscripts

p	p-type
n	n-type

estimation of interactions between the fluid sources and the generators and are able to suggest general strategies for the aforementioned optimization. However, simplified fluid models are not sufficient to accurately predict the detailed behavior of most practical fluid systems with multidimensional construction, irregular geometry, dynamic variations in mass flow, or complicated combustion processes, nor can they precisely transfer nonuniform heat flow and temperature distributions to the thermoelectric model as the boundary condition. On the other hand, the assumption of constant material properties made in the analytical thermoelectric model is not realistic in many applications. For thermal fluid tubes and fuel fired combustors on which thermoelectric generators can be mounted, the temperature therein is high, ranging from hundreds to more than one thousand degree. Thus the values of the three principal properties of the p-type and n-type materials, i.e., $\alpha_{p,n}$, $\rho_{p,n}$, and $k_{p,n}$, will strongly vary with temperature.

The nonlinearity in thermoelectric device modeling due to the temperature dependency of material properties in most cases necessitates a numerical approximation instead of analytical methods, whereas complicated fluid power systems can be simulated using available computational fluid dynamics (CFD) techniques. Particularly, a number of CFD models have been developed [15,30–34] to deal with the thermoelectric generation by FLUENT, a widely used industry code. However, these CFD models only simulate the status of heat source fluids or convection/radiation effects on thermoelements without an appropriate model of thermoelectric generators. In other recent works, both FLUENT and thermoelectric generator simulation have been employed to study the system thermal behavior, but coupling of the two numerical programs has not been completed, i.e., the interaction is in a single direction [35,36]. Although in principle, numerical heat transfer schemes of thermoelectricity, such as the model in the commercially available finite element method (FEM) program ANSYS [37] (used in [35]), the one used in [36], and those described in [38–40], can be linked to a CFD simulator through a relaxation strategy, auxiliary coding is usually required for iteration control, data transfer, and synchronization between different simulators. The processing of coupling relationships of multidimensional boundary values for the same model domain but with different simulators may be especially difficult [41]. Therefore, it is certainly preferable to model both fluid behaviors and thermoelectric power output with the same tool to minimize the number of simulators with high usability and without loss of accuracy.

This work presents a three-dimensional (3D) numerical solution to the fluid-structure coupled problem by implementing a FLUENT compatible thermoelectric model. FLUENT and its user-defined functions (UDFs) were selected for fuel cells to model the electrochemical reactions and the electric field caused by the Nernst potential throughout the cell [42]. The most significant benefit of using FLUENT to model such power sources is that the existing knowledge/experience of this computational tool and the innumerous fluid models already implemented by it can be efficiently utilized to predict the coupled system performance. Moreover, UDFs allow for a convenient customization and enhancement of FLUENT, where the thermoelectric device model can be connected to the thermal fluid model as a continuum domain to avoid boundary-value transport problems, making the co-design of the thermoelectric generator and fluid heat sources simpler and less time-consuming. In the following sections of this paper, 3D governing equations and the general multidimensional numerical algorithm of thermoelectric generation, model implementation in FLUENT, and model results, will be described.

2. Multidimensional multiphysics numerical scheme

A typical thermoelectric power system is shown in Fig. A.1, in which many n- and p-type semiconductor legs composing the generator are connected thermally in parallel between the hot and cold fluid sources and electrically in series to power the load circuit. Details of the general numerical algorithm used to deal with nonlinear issues such as heat production due to the Joule effect, unsteady state conduction, and temperature dependent material properties in one-dimensional (1D) transport equations for such thermoelectric generators were documented in a previous study [43], in which we introduced a combined finite difference and Newton–Raphson method based on the governing equation system from the energy conservation theory. The main intention of Section 2 is to extend the 1D algorithm to the multidimensional implementation of the multiphysics numerical scheme for thermoelectric generators operating in thermal fluids.

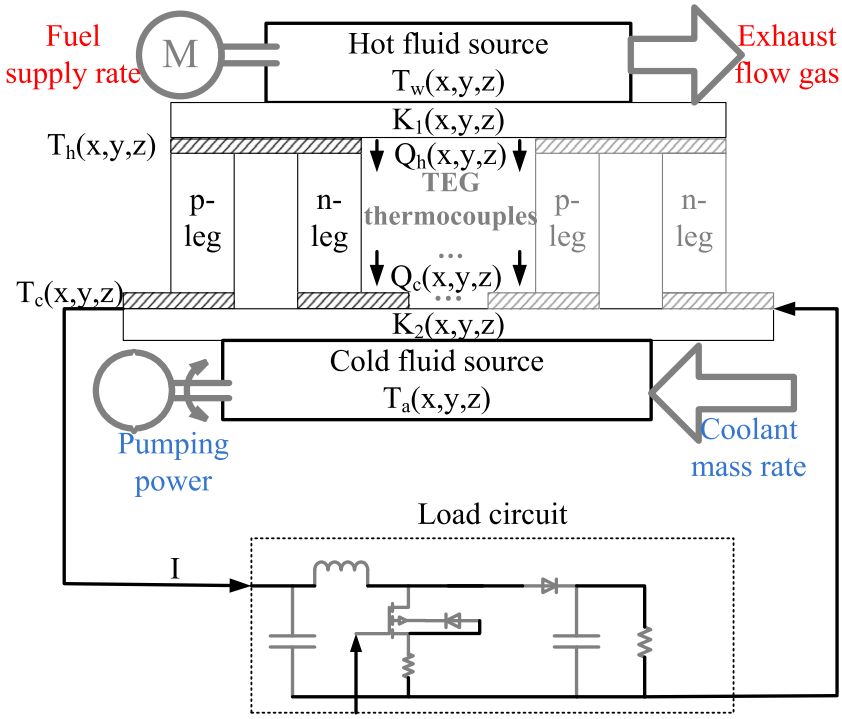

Fig. A.1. Schematic representation of a typical fluid–thermal–electric-circuit coupled power system.

As is shown in Fig. A.1, it is clear that, for fluid heat sources with flowing mass, neither their temperature nor their heat flow profiles along the contact interface to thermoelectric generators can be uniform. Obviously the results of the thermal analysis are now multidimensional, e.g., the temperature and heat flow distribution should be expressed as $T_{p,n}(x,y,z)$ and $q_{p,n}(x,y,z)$ in a 3D model, respectively. In the case of temperature dependent material properties, neglecting the side heat loss outside the solid legs, the 3D governing equation of the thermal field inside a control volume is written as,

$$\nabla q_{p,n} = -\nabla[k_{p,n}(T_{p,n})\nabla T_{p,n}] = m_{p,n}c_{p,n}\frac{\partial T_{p,n}}{\partial t} + J^2\rho_{p,n}(T_{p,n}) + [\nabla\alpha_{p,n}(T_{p,n})]T_{p,n}J, \quad (1)$$

where the first term in the right side is the transient term, the second term is the temperature dependent Joule electrical energy production, and the third source term represents the contributions from Peltier (inhomogeneous or segmented materials) and Thomson effects. By an electro-thermal analogy, the heat transfer governed by (1) is illustrated in Fig. A.2 (a), a control volume of the 3D thermal resistor network.

The electrical analysis requires these thermal analysis results, mainly the temperature profiles, to find the total Seebeck voltage generated and the temperature dependent material properties. Keeping the non-ohmic current–voltage relation in both legs of the device in mind [44], the governing equation of the electric field inside a control volume under steady state is written as,

$$\nabla V = -\alpha_{p,n}(T_{p,n})\nabla T_{p,n} - \rho_{p,n}(T_{p,n})J, \quad (2)$$

where the first term in the right side of (2) is the Seebeck electromotive force (EMF) increase due to the temperature gradient, and the second term is the voltage drop due to the current flowing through the control volume. As a result of the 3D temperature distribution, the electric current and potential distribution are also 3D, i.e., $J(x,y,z)$ and $V(x,y,z)$. In addition, the values of $R_{p,n}$ must be obtained by a calculation of a 3D resistor network for the 3D resistivities $\rho_{p,n}(x,y,z)$, which is shown in Fig. A.2 (b), where the current

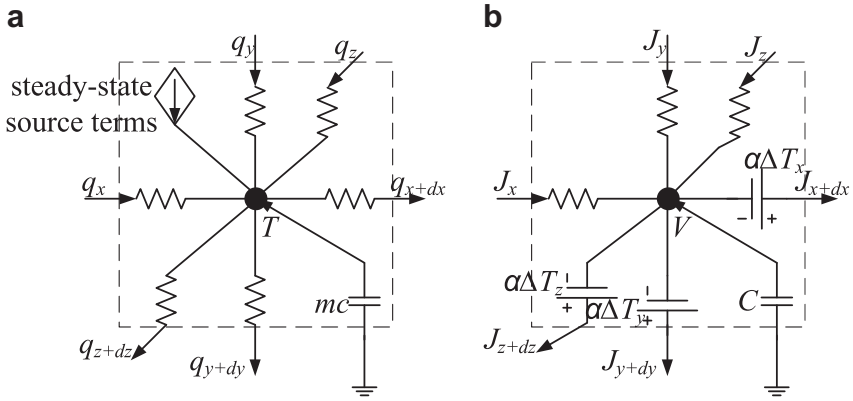

Fig. A.2. A control volume of (a) 3D thermal resistor network Eq. (1), (b) 3D electric resistor network Eq. (2).

vector flows in three directions against the Seebeck voltage sources. Although the 1D analysis is fast and easy to manipulate, it lacks details about the lateral distributions of electric potential and current, and hence, it is impossible to obtain the effective electrical resistance. Therefore, the 3D electric field analysis of thermoelectric generators, by which the main results of power and efficiency can be obtained, should be accompanied by the 3D thermal field analysis.

The complete solution of a multidimensional multiphysics problem relies on a clear data and algorithm flow chart, in which various numerical approximation methods for the nonlinear differential equation system can be identified and connected as a sequential process. Fig. A.3 shows such a self-consistent flow chart for thermoelectric generators operating in the system mode as shown in Fig. A.1. The basic mechanism consists of four simulation modules: a 3D CFD simulation is used for the energy and mass transfer status in the hot and cold fluid domains; a 3D thermal simulation for the temperature and heat conduction distribution in the thermoelectric domain; a 3D electric simulation for the electric field distribution and electric conduction in the thermoelectric domain; and a 1D circuit simulation for the current and power performance of the actual load. The four simulation modules are coupled together and there are three direct coupling relationships among them. First, the CFD simulation is coupled with the thermoelectric thermal simulation through the contact boundary, that is, the 3D boundary temperature and heat flux of both the fluid domains and the solid domain should be kept continuous with each other as a whole. Second, within the thermoelectric device, the thermal simulation and the electric simulation are coupled with each other over the entire 3D solid domain through the update of all of the temperature dependent material properties, the temperature distribution, and the current density. Third, the 3D electric simulation is coupled with the load circuit as a field-circuit coupling, where the overall Seebeck voltage and effective internal resistance, calculated from the 3D electric simulation, are applied as a DC voltage source to the external load circuit.

Unlike the thermoelectric power source, the load's current–voltage relation fulfills Ohm's law, and there is no need to consider the power output in a 3D way. Depending on the position of the electrode pads of the actual device, the translation between the 3D current distribution from the thermoelectric electric simulation and the 1D current from the circuit simulation can be easily carried out because the current is the only boundary condition in this field-circuit coupling. For the coupling between the fluid field and the thermoelectric field, however, the boundary condition translation is much more difficult because the CFD simulation and the thermoelectric thermal simulation both output 3D heat flow and temperature distributions at the boundary surface. There are two boundary conditions for the same boundary domain, and one of them must be known beforehand for both simulators to start the thermal simulations. Fig. A.3 shows one iteration strategy, where initial values of the boundary heat flow distribution $Q_{h,c}(x,y,z)$ must be given before the CFD simulation starts to run. Then, the temperature distribution $T_{w,a}(x,y,z)$, as the solution of the energy transfer equations solved in the CFD simulation, can be used in the numerical thermal analysis of the thermoelectric field, whose analysis results are fed back to the CFD simulation to update $Q_{h,c}(x,y,z)$ as the new boundary values.

In spite of the iteration instance, the translation of the multidimensional thermal boundary condition in practical simulation usually involves complicated mathematics and computational technique, as shown in [41] and other open reports. To avoid any theoretical difficulties brought about by such a manipulation between CFD and heat transfer simulators, it is advantageous to implement the thermoelectric model in the CFD framework as well; thus, the solid and the fluids are defined in a continuum zone and the boundary is simply solved as interior nodes by a single solver. The next section will present the detailed treatment of thermoelectric modeling in FLUENT to enable an efficient fluid-thermal-electric coupled simulation as the scheme displayed in Fig. A.3. The resistance of the load circuit is extracted and used in the thermoelectric modeling such that the field-circuit coupling is also included to some extent.

3. Numerical model

The 3D thermoelectric generator model is implemented in FLUENT 6.3, a finite volume method (FVM) CFD package, in which the solid thermoelectric phenomena and the algorithm described in Fig. A.3 are taken into account by developing UDF through ANSI-C language. The model serves as an add on module in parallel with other power source modules [42] provided within the standard FLUENT software.

Meshing of the GAMBIT pre-processor of FLUENT is applied to leg volumes in which tetrahedral elements are dominant in this work, but one may of course use other meshers and element types if the device under study has irregular leg shapes. The grid generated is read into the FLUENT solver and scaled to align the geometrical units. Both the thermal analysis and the electric analysis use the same grid, and thus, they have the same 3D coordinate system with regard to the cells and boundary walls of the leg volumes.

FLUENT has the ability to compute the conduction of heat through solids when the Energy Model is activated. Temperature dependent thermal conductivities can be specified by polynomial functions and assigned to *p*- and *n*-leg cell zones for *p*- and *n*-type

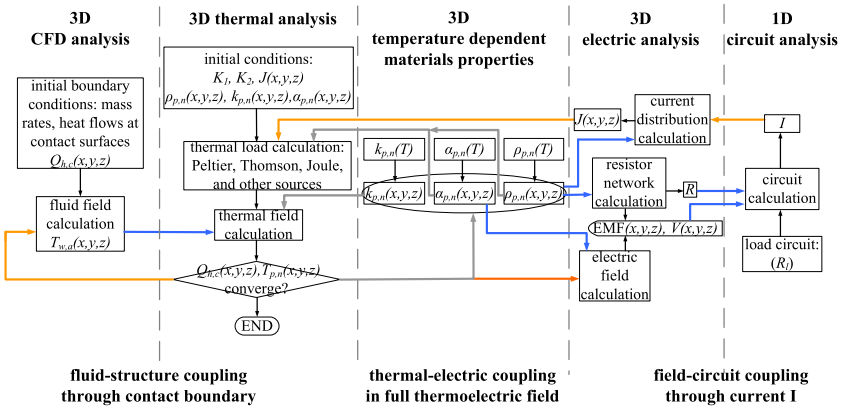

Fig. A.3. Energy conservation based multidimensional multiphysics simulation procedure for thermoelectric fluid power systems.

materials, respectively. The thermal boundary condition of the thermoelectric generator does not need to be specified in the system modeling because it will be solved in terms of fluid system boundary conditions, and all aspects of fluid flow, heat and mass transfer in heat sources are handled by FLUENT. The transient source term in (1) can also be included automatically with appropriate settings in FLUENT. The values of Joule, Thomson, and Peltier, i.e., steady state source terms, however, rely on the 3D electric analysis results, as shown in (1) and Fig. A.3. Thus an electric field solution is required to complete the thermal field calculation.

FLUENT solves generic transport equations for user defined scalars (UDS) which can be used to determine the electric field in a CFD environment. The difficulty herein is that the governing Eq. (2) is not in the generic transport equation form due to the Seebeck EMF. To correctly write (2) for the solver, two UDS are used to represent the two terms in the right side of (2). UDS0 is used to represent the 3D potential distribution of the ohmic voltage drop caused by the current vector,

$$\nabla \mathrm{UDS0} = -\rho_{p,n}(T_{p,n})J. \tag{3}$$

Solving for 3D electrical conduction is directly analogous to the computation of heat transfer. The field throughout the conductive regions is calculated based on flux (charge) conservation in each cell,

$$\nabla J = 0, \tag{4}$$

so we have

$$\nabla\left[-\frac{1}{\rho_{p,n}(T_{p,n})}\nabla \mathrm{UDS0}\right] = 0. \tag{5}$$

FLUENT solves this Laplace equation for the potential field by enforcing a specific flux J on one boundary wall of both p- and n-type solid regions and zero potential on the other boundary wall to represent the ground, where the I value of the present iteration is the basis on which the specific J distribution on the UDS0 boundary is calculated. The temperature dependent electrical conductivities $1/\rho_{p,n}(T_{p,n})$ are specified as the diffusivities of UDS0 by polynomial functions for p- and n-type materials. Referring to Fig. A.3, the functions of the resistor network calculation and current distribution calculation are both implemented in terms of UDS0.

UDS1 is used to represent the 3D Seebeck EMF distribution produced by the temperature field,

$$-\nabla \mathrm{UDS1} = \alpha_{p,n}(T_{p,n})\nabla T_{p,n}, \tag{6}$$

whose divergence is

$$\nabla(-\nabla \mathrm{UDS1}) = \nabla[\alpha_{p,n}(T_{p,n})\nabla T_{p,n}]. \tag{7}$$

If we take an unit diffusivity for UDS1, (7) becomes a generic transport equation where the right side can be assumed to be the source term, although it does not have a real physical meaning as a source in the thermoelectric modeling. The setting of the boundary conditions for UDS1 is the same as that for UDS0 except that a constant value is used to calculate the flux J instead of I. Thus, the electric field calculation function in Fig. A.3 can be implemented with regard to UDS1 if the source term is appropriately included.

Before proceeding to the implementation of the right side of (7), we recall the source term in the 3D thermal Eq. (1). An energy_source UDF is written to modify the heat conduction computation to include the Joule, Thomson, and Peltier heating. FLUENT calls the UDF as it performs a global loop on cells to compute the source term and returns it to the solver. Because the current distribution calculation has been done with UDS0, the Joule source term can be easily obtained. In the practical implementation, the Joule heat can be calculated as the product of the sum of the squares of vector components of the gradient of UDS0 and the temperature dependent electrical conductivity,

$$J^2\rho_{p,n}(T_{p,n}) = \frac{1}{\rho_{p,n}(T_{p,n})}(\nabla \mathrm{UDS0})^2 = \frac{1}{\rho_{p,n}(T_{p,n})}\left[\left(\frac{\partial \mathrm{UDS0}}{\partial x}\right)^2 + \left(\frac{\partial \mathrm{UDS0}}{\partial y}\right)^2 + \left(\frac{\partial \mathrm{UDS0}}{\partial z}\right)^2\right]. \tag{8}$$

The source terms of Thomson and Peltier (in the case of inhomogeneous or segmented materials) in each cell involve the gradient of the Seebeck coefficient $\alpha_{p,n}$. To express $\nabla\alpha_{p,n}(T_{p,n})$ for the source term, UDS2 is used to represent the scalar of $\alpha_{p,n}(T_{p,n})$. We constitute a transport equation for UDS2,

$$\nabla(-\nabla \mathrm{UDS2}) = 0, \tag{9}$$

where a unit diffusivity for UDS2 is taken. It should be remarked that the result for UDS2 from the solver is not interesting because (9) does not hold any physical meaning. Instead, once per iteration, an at_end UDF is executed to fill UDS2 with the local Seebeck coefficient $\alpha_{p,n}(T_{p,n})$ according to the temperature $T_{p,n}(x,y,z)$ for each cell. The solved scalar field for UDS2 is replaced therein, where temperature dependent Seebeck coefficients are specified in the UDF by polynomial functions for p- and n-type materials, respectively. If we substitute ∇UDS2 into the source term of Thomson and Peltier in (1), we obtain the thermoelectric source term,

$$[\nabla\alpha_{p,n}(T_{p,n})]T_{p,n}J = -\nabla \mathrm{UDS2}\frac{T_{p,n}}{\rho_{p,n}(T_{p,n})}\nabla \mathrm{UDS0}. \tag{10}$$

It consists of three components,

$$\left[\frac{\partial\alpha_{p,n}(T_{p,n})}{\partial x}\right]T_{p,n}J_x = -\frac{\partial \mathrm{UDS2}}{\partial x}\frac{T_{p,n}}{\rho_{p,n}(T_{p,n})}\frac{\partial \mathrm{UDS0}}{\partial x}, \tag{11a}$$

$$\left[\frac{\partial\alpha_{p,n}(T_{p,n})}{\partial y}\right]T_{p,n}J_y = -\frac{\partial \mathrm{UDS2}}{\partial y}\frac{T_{p,n}}{\rho_{p,n}(T_{p,n})}\frac{\partial \mathrm{UDS0}}{\partial y}, \tag{11b}$$

$$\left[\frac{\partial\alpha_{p,n}(T_{p,n})}{\partial z}\right]T_{p,n}J_z = -\frac{\partial \mathrm{UDS2}}{\partial z}\frac{T_{p,n}}{\rho_{p,n}(T_{p,n})}\frac{\partial \mathrm{UDS0}}{\partial z}, \tag{11c}$$

all of which are included in the sum of the energy_source UDF.

Now we proceed to the source term in (7) for UDS1, implemented by an UDS1_source UDF,

Table A.1
Transport equation parameters of scalar fields.

.	Diffusivity	Source term	Top wall boundary	Bottom wall boundary
UDS0.	$\frac{1}{\rho_{p,n}(T_{p,n})}$	0	specified flux (I)	specified potential (0)
UDS1.	1	UDS1_source UDF	specified flux (0)	specified potential (0)
UDS2.	1	0	specified flux (0)	specified potential (0)
UDS3.	1	0	specified flux (0)	specified potential (0)
UDS4.	1	0	specified flux (0)	specified potential (0)
UDS5.	1	0	specified flux (0)	specified potential (0)
Temperature.	$k_{p,n}(T_{p,n})$	energy_source UDF	from CFD	from CFD

$$\nabla[\alpha_{p,n}(T_{p,n})\nabla T_{p,n}] = \frac{\partial \alpha_{p,n}(T_{p,n})\frac{\partial T_{p,n}}{\partial x}}{\partial x} + \frac{\partial \alpha_{p,n}(T_{p,n})\frac{\partial T_{p,n}}{\partial y}}{\partial y} + \frac{\partial \alpha_{p,n}(T_{p,n})\frac{\partial T_{p,n}}{\partial z}}{\partial z}. \quad (12)$$

To express the above equation in the UDF, UDS3, UDS4, and UDS5 are used to represent $\alpha_{p,n}(T_{p,n})\frac{\partial T_{p,n}}{\partial x}$, $\alpha_{p,n}(T_{p,n})\frac{\partial T_{p,n}}{\partial y}$, and $\alpha_{p,n}(T_{p,n})\frac{\partial T_{p,n}}{\partial z}$, respectively, as three scalar fields. Similarly to UDS2, we constitute transport equations for these scalars,

$$\nabla(-\nabla \mathrm{UDS3}) = 0, \quad (13a)$$

$$\nabla(-\nabla \mathrm{UDS4}) = 0, \quad (13b)$$

$$\nabla(-\nabla \mathrm{UDS5}) = 0, \quad (13c)$$

not for their solutions from FLUENT but to fill them with products of the temperature dependent Seebeck coefficient and the three

Table A.2
Comparison of 1D simulation results, T_h = 423 K, T_c = 303 K.

Quantity	Analytical	ANSYS	FLUENT coarse grid	FLUENT medium grid	FLUENT refined grid	Measurement
Q_h, W	81.3	83.29	80	81.6	81.8	70
P, W	3.98	3.76	3.08	3.57	3.62	2.51
η%	4.89	4.51	3.85	4.38	4.43	3.6
I, A	1.08	1.05	0.952	1.024	1.032	0.86

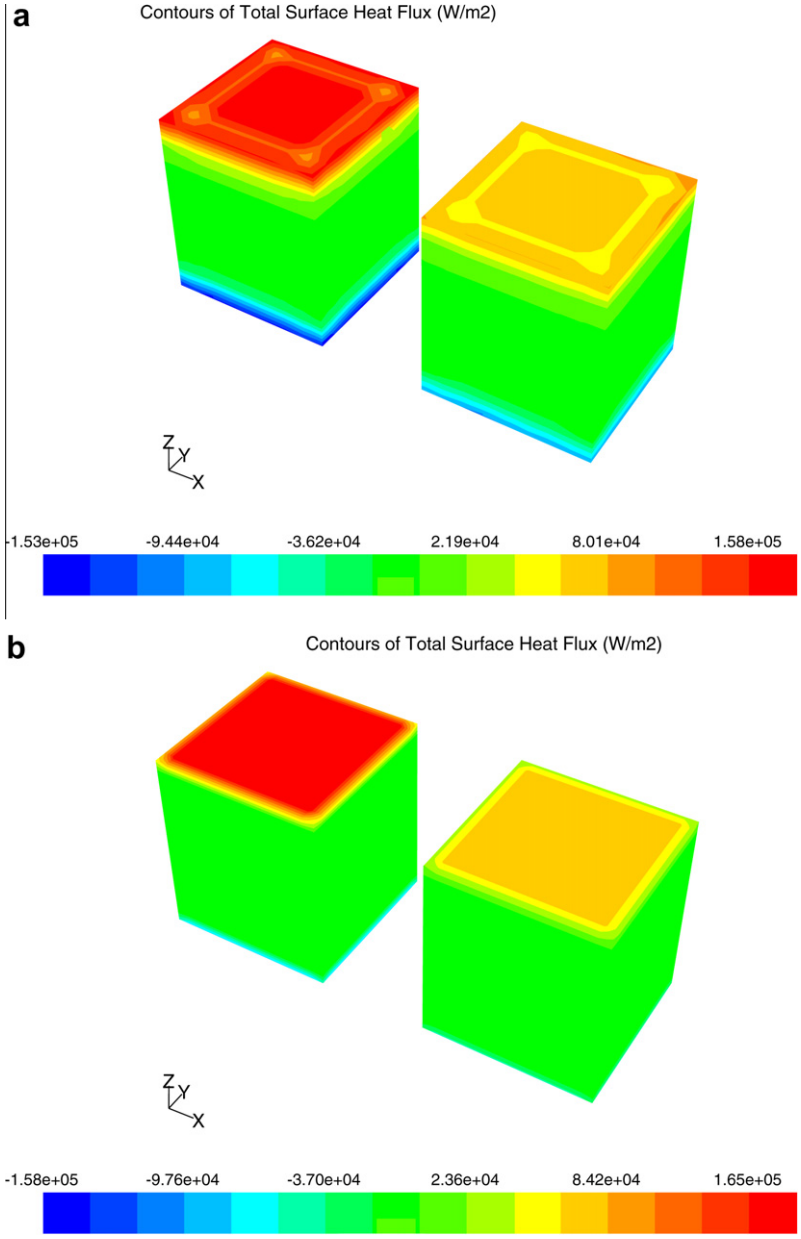

Fig. A.4. Simulation of surface heat flux (W/m^2) distributions. T_h and T_c are 423 K and 303 K, respectively. (a) using the coarse grid. (b) using the refined grid.

components of the temperature gradient in the at_end UDF. Because the gradients of UDS3, UDS4, and UDS5 can be accessed, the source term (12) for UDS1 is appropriately implemented.

At the end of every iteration (at_end UDF), both the ohmic voltage drop represented by UDS0 and the Seebeck EMF represented by UDS1 are determined. Their spatial addition in terms of (2) in the full solid region gives the 3D potential distribution $V(x,y,z)$, and the effective internal resistance of the legs, R_p and R_n, can also be calculated. Including the load R_l, the new value of I is

$$I = \frac{\mathrm{UDS1}_p - \mathrm{UDS1}_n}{R_p + R_n + R_l}, \tag{14}$$

which will be used in the next iteration as the boundary condition for UDS0. $\mathrm{UDS1}_{p,n}$ is the total built-in Seebeck EMF of the leg, which should be equivalent to the open circuit voltage at no load. This calculation is relevant to the position of the actual electrodes at which I is applied, but in this work, the UDS1 potential of the boundary wall is simply used. The previous 1D study [43] aims for the co-design in which the thermoelectric generator system is associated with complicated electrical systems. For the 3D FLUENT model, if R_l can emulate the input impedance of the load circuit, the aforementioned field-circuit coupling is also included.

As far as can be observed, all thermoelectric function modules in Fig. A.3 are implemented by UDF and UDS. The boundary condition, diffusivity, and source term of the UDS and temperature fields are summarized in Table A.1. The model can be easily implemented for practical devices with multiple thermocouples. When the boundary walls of the legs are coupled with the fluid flows, thermal boundary conditions are no longer required on them because FLUENT will calculate the heat transfer directly from the solution in the adjacent cells of both sides. The iteration is automatically done by FLUENT until convergence is achieved.

4. Model results

First, a comparison of the 1D steady-state simulation between the FVM FLUENT and FEM ANSYS [37] is carried out to theoretically validate the proposed model. The example considered is the performance of the thermoelectric generator described in the previous study [43], the TEC1-12706 thermoelectric module made by Tianjin Institute of Power Sources, China, which was chosen for the experimental validation therein. The element length is $L = 1.6$ mm for both the p-type and n-type semiconductors, and the element cross-sectional areas are $S_p = S_n = 1.4 \times 1.4\ \mathrm{mm}^2$. The generator has 127 thermocouples and is connected to a linear load resistance $R_l = 3.4\Omega$. Second, third, or fourth order polynomial functions are used to fit the temperature dependency of the p-type and n-type material properties.

Initially, the constant temperature boundary condition is set on the top and bottom surfaces for the 1D simulation, where zero heat loss from the other four sides of the legs is assumed. With the temperature polynomial functions used for varying material properties, the FLUENT thermoelectric model is performed to analyze Q_h, P, η, and I for the generator operating between $T_c = 303$ K and $T_h = 423$ K. A gird sensitivity analysis is performed for the presented FLUENT model to check its gird independency, where three grid schemes used in the computation are designated as a coarse grid, a medium grid, and a refined grid, respectively. The parameters computed by FLUENT with the three grids and ANSYS as well as the analysis using the material properties evaluated at an

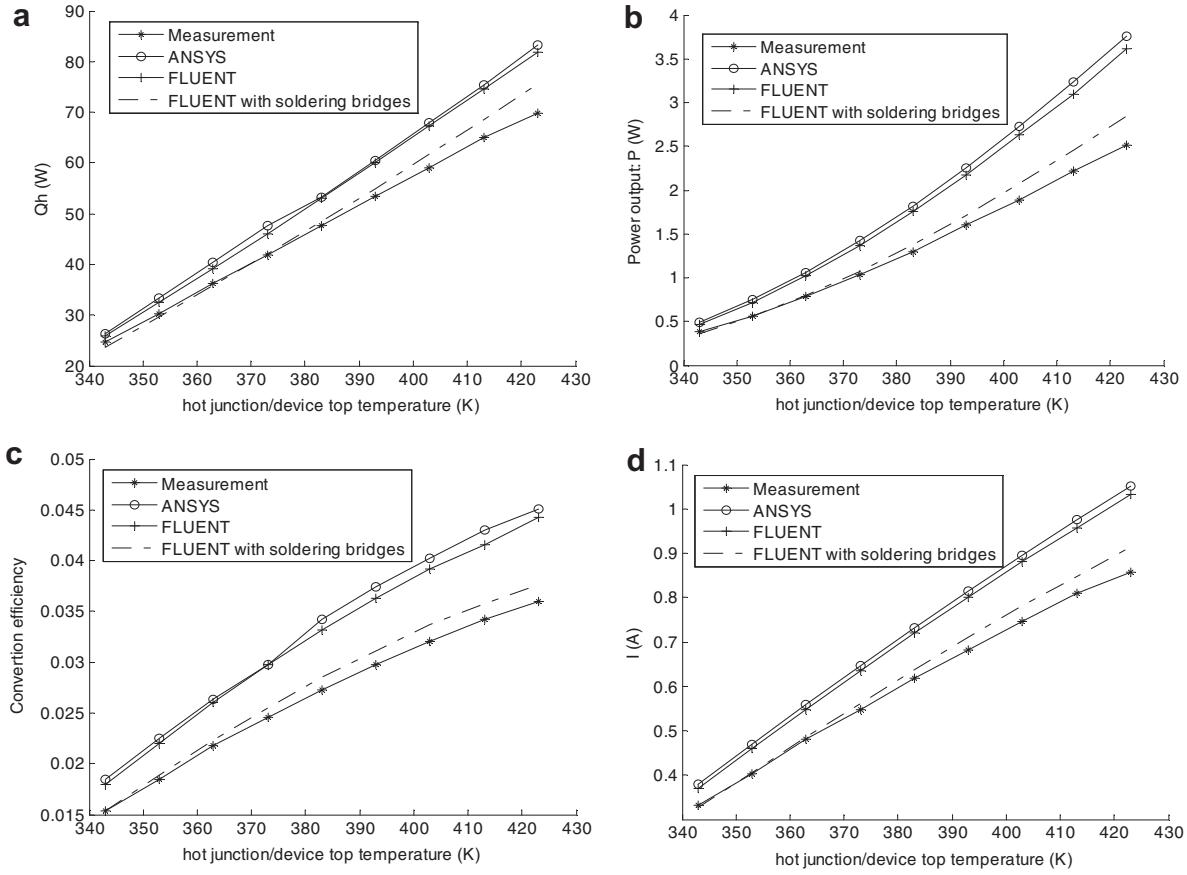

Fig. A.5. Comparison between simulation and measured results for various temperature difference. Cold junction/device bottom temperature is fixed at 303 K, $R_l = 3.4\Omega$. (a) Q_h, (b) P, (c) η, and (d) I.

average temperature of 363 K are summarized in Table A.2. The experimental data collected in [43] are also provided for comparison. Clearly, the analytical model is essentially less realistic than the numerical models and yields a higher η if average material properties are used rather than the temperature dependent material properties. This result has been pointed out in [37], where the cause of the efficiency decrease is mainly the heat evolution of the Thomson effect. When the grid is sufficiently dense, FLUENT can output almost exactly the same results as those achieved by ANSYS. The discrepancy caused by the relatively coarse grid attributes to the inherent multidimensional features of FLUENT. In Fig. A.4, it can be seen that the nonuniformity of the surface heat transfer contributing to the interior conduction in the legs of a single couple is appreciable. When the grid becomes dense enough, the discreteness error is minimized, as shown in Fig. A.4 (b). For the refined grid, the convergent simulation results of FLUENT and ANSYS under different temperature spans are shown in Fig. A.5, where numerical results of the performance parameters from both models display almost the same characteristics in this 1D case.

To illustrate how the surface heat loss can produce multidimensional effects, the 3D temperature and electric potential distributions in the thermocouple by the FLUENT model are depicted in Figs. A.6, A.7 (a), where all leg surfaces except the top and bottom junctions are assumed to be exposed to heat transfer with a coefficient of 500 W/m^2 K, representing contributions from both natural convection and radiation heat transfer. The bulk mean temperature in the module cavity is set to be the arithmetic average of T_h and T_c. i.e., 363 K. With the same model parameters, in Figs. A.6, A.7 (b) 3D simulation results of ANSYS show a qualitative agreement with the contours from the FLUENT model. For a quantitative comparison, the performance parameters are calculated for both models. Due to the prescribed temperature boundary condition on the legs, it is found that the influence of surface heat loss on P and I is negligible in this case. However, with the surface heat

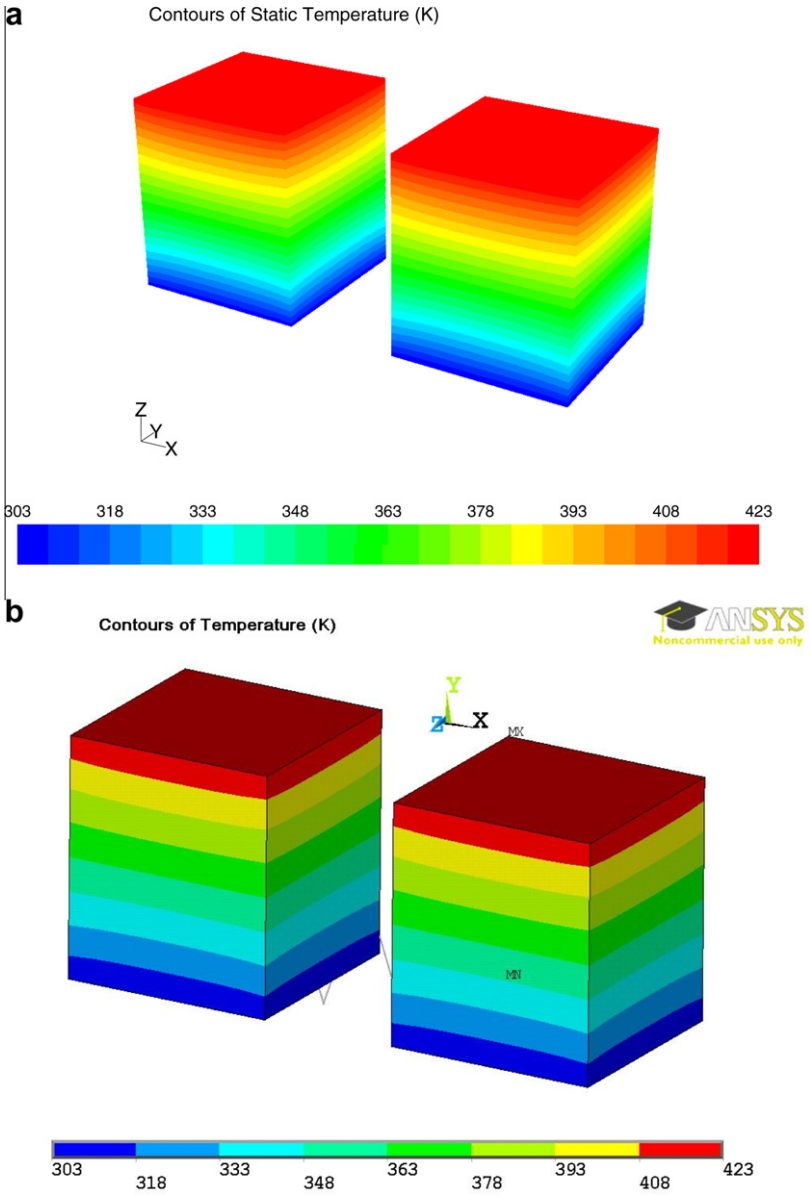

Fig. A.6. Simulation of temperature (K) distributions for a convection heat transfer coefficient of 500 W/m^2 K. T_h and T_c are 423 K and 303 K, respectively. (a) FLUENT, (b) ANSYS.

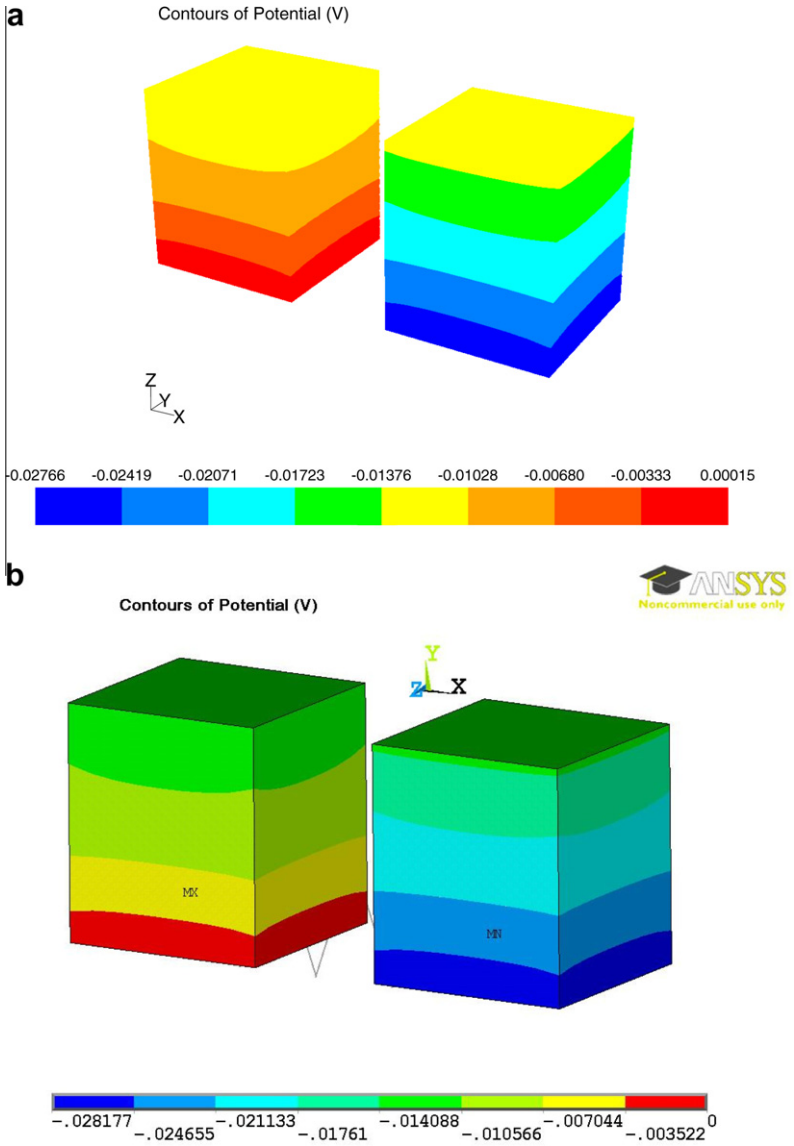

Fig. A.7. Simulation of electric potential (addition of Ohm's and Seebeck potential, V) distributions for a convection heat transfer coefficient of 500 W/m^2 K. T_h and T_c are 423 K and 303 K, respectively. The cold junction of the p-type (left) leg of the thermocouple is prescribed as ground in this postprocessing, and a scaled load (R_l/127) is assumed connected between the cold junctions of the p-type and n-type legs. (a) FLUENT, (b) ANSYS.

loss, Q_h is significantly increased to maintain the original temperature difference, and hence η is decreased. The changes in Q_h and η with different heat transfer coefficients are plotted in the close-up of Fig. A.8, where both numerical models display almost the same characteristics again in the case of surface heat loss.

For the device example modeled, the influence of the non-ideal effects of the thermal and electrical interface resistances on performance parameters turns out to be obvious in the 1D study [43]. These interface resistances are re-modeled three-dimensionally in conjunction with the nonuniform temperature boundary condition across the intermediate components of the soldering bridges. The detailed profile of the vertical thermal power of the solid model is shown in Fig. A.9. The thermal and electrical interface resistances, and the Joule heat of the electrical interface resistance are all included in the top and bottom bridges, although the last has only tiny effects in this case. At the hot and cold faces of the thermoelements the heat conduction has a sudden change in the vertical direction, reflecting the Peltier heat absorbed and evolved at the junctions of dissimilar materials. This reversible heat is automatically taken into account by the thermoelectric source term described in Section 3.

The key performance parameters calculated by the model with soldering bridges are also shown in Fig. A.5 for comparison. Although there are still some differences between the simulated and measured results in the high temperature range after the true 3D interface is modeled, it can be seen in Fig. A.5 that the simulation data match the real measurement closely, with a good correlation. The acceptable deviation has been analyzed and can be mainly attributed to the non-ideal accuracy of the heat flow determination in the device test rig and the inherent uncertainties of the commercial thermoelectric module [43]. However, the negligible discrepancy between the numerical models validates the proposed CFD model as a thermoelectric simulator equivalent to ANSYS, and to the other numerical model introduced in [43] in 1D cases. Given that the experimental determination of thermal quantities (such as conductivity) in most measurements has errors of a similar level, the FLUENT model has been able to predict the efficiency and output power of thermoelectric generators operating in fluid systems

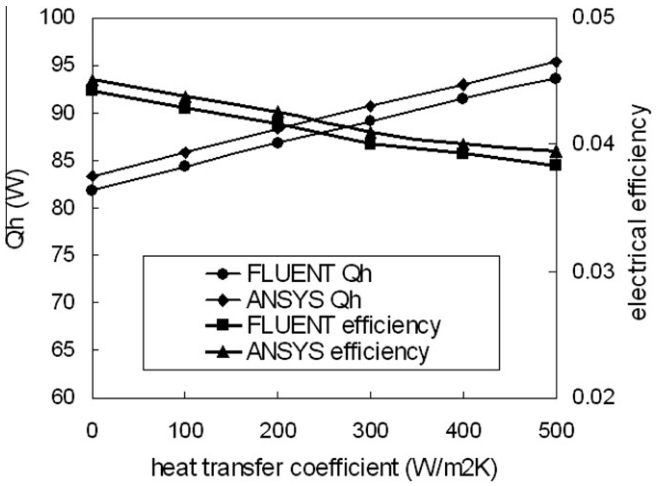

Fig. A.8. Comparison of input heat flow and conversion efficiency between FLUENT and ANSYS simulations for various convection heat transfer coefficients. T_h and T_c are 423 K and 303 K, respectively.

with sufficient accuracy. Further refining work will focus on improving the accuracy of parameter acquisition in the test rig for the model, where more advanced modules will be measured under hot sources of higher temperature.

5. Conclusions

(i) The thermoelectric processes of Seebeck, Peltier, and Thomson effects are integrated with Joule source terms through a FVM numerical scheme into a CFD simulator. The proposed FLUENT model includes the temperature dependence of all properties of the *p*- and *n*-type materials composing the thermocouple. The 3D modeling results provide detailed profiles of temperature, Seebeck potential, and current density as well as the values of power and efficiency. Comparisons to other modeling and experimental results validate the accuracy of the numerical model.

(ii) The functionality of solving scalar fields in the CFD simulator has been extended for the potential field in solid zones of thermoelectric generators. The power source model is comprised of only several UDF and UDS, and hence, it is scalable and flexible for loading in FLUENT to interact with CFD submodels, and especially useful in the design of entire power systems with 3D temperature and heat flux profiles [45]. The numerous existing CFD models of fluid flow and combustion in FLUENT can be immediately connected to the thermoelectric model as a continuum domain, where the difficulties encountered in the implementation of the multi-dimensional boundary condition translation of the fluid-structure coupling are avoided. To handle the field-circuit interface, a general flux computation is defined in terms of the load and incorporated into the UDS boundary.

(iii) One important feature of the present model is the incorporation of the reversible contributions from inhomogeneous materials and the Thomson effect into the source term of heat conduction. In particular, the thermal flux in the computational results expresses the usual conduction heat flow, and thus, it has a direct connection with the temperature field and can be studied separately from the reversible Peltier and Thomson heat. This function is not available in ANSYS, in which the reversible heat and the irreversible conduction are inextricable in the total heat flow. Such treatment of the present model makes relevant simulation results easier to analyze and to truly understand as compared to other numerical models in which irreversible and reversible heat are defined together [37,40], and offers a new option for studying the effects of the Thomson heat.

(iv) Not only can 3D calculations in the thermoelectric generator model aid in optimizing the selection of the 3D shape and geometry of a device, the effects of various convection and radiation conditions on power performance, especially in the case of porous medium, can also be easily studied by the model due to the inherent CFD advantages of FLUENT in modeling and implementing such source terms. Besides, the 3D FLUENT model is able to treat both isotropic and

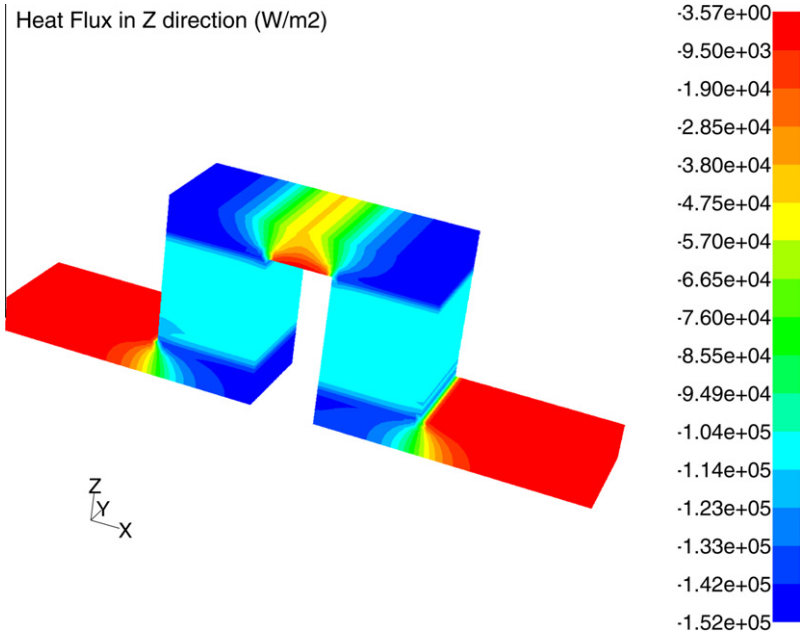

Fig. A.9. Simulation of vertical heat flux (W/m^2 in *Z* axis) with soldering bridges. Device top and bottom are 423 K and 303 K, respectively. Peltier heat's contribution to the interior conduction is included automatically by the model.

orthotropic physical and thermoelectric properties provided that such a study becomes mandatory to the overall system behavior.

Acknowledgments

This work is funded in part by the Danish Council for Strategic Research, Programme Commission on Energy and Environment, under Grant No 2104-07-0053, and is carried out in the Center for Energy Materials in collaboration with Aarhus University, Denmark. The authors are grateful to Peter Naamansen who helped them with constructive discussions.

Appendix A. Supplementary materials

A computational case and the UDF library associated with the proposed model can be found in the on-line version as the supplementary data to operate in Fluent 12 directly. Supplementary data associated with this article can be found, in the online version, at doi:10.1016/j.ijheatmasstransfer.2010.08.024.

References

[1] E.F. Thacher, B.T. Helenbrook, M.A. Karri, C.J. Richter, Testing an automobile thermoelectric exhaust based thermoelectric generator in a light truck, Proc. IMechE. D: J. Automob. Eng. 221 (2007) 95–107.
[2] A. Killander, J.C. Bass, A stove-top generator for cold areas, in: Proceedings of 15th International Conference on Thermoelectrics, Pasadena, USA, 1996, pp. 390–393.
[3] R.Y. Nuwayhid, A. Shihadeh, N. Ghaddar, Development and testing of a domestic woodstove thermoelectric generator with natural convection cooling, Energ. Convers. Manag. 46 (2005) 1631–1643.
[4] W. Moser, G. Friedl, W. Haslinger, H. Hofbauer, Small-scale pellet boiler with thermoelectric generator, in: Proceedings of 25th International Conference on Thermoelectrics, Vienna, 2006, pp. 349–353.
[5] C. Lertsatitthanakorn, Electrical performance analysis and economic evaluation of combined biomass cook stove thermoelectric (BITE) generator, Bioresour. Tech. 98 (2007) 1670–1674.
[6] K. Qiu, A.C.S. Hayden, Development of a thermoelectric self-powered residential heating system, J. Power. Sources 180 (2008) 884–889.
[7] S.B. Schaevitz, A.J. Franz, K.F. Jensen, M.A. Schmidt, A combustion-based MEMS thermoelectric power generator, in: Proceedings of 11th International Conference on Solid-State Sensors and Actuators, Munich, Germany, 2001, pp. 30–33.
[8] C. Zhang, K. Najafi, L.P. Bernal, P.D. Washabaugh, An integrated combustor-thermoelectric micro power generator, in: Proceedings of 11th International Conference on Solid-State Sensors and Actuators, Munich, Germany, 2001, pp. 34–37.
[9] J. Vican, B.F. Gajdeczko, F.L. Dryer, D.L. Milius, I.A. Aksay, R.A. Yetter, Development of a microreactor as a thermal source for microelectromechanical systems power generation, Proc. Combust. Inst. 29 (2002) 909–916.
[10] R. Funahashi, T. Mihara, M. Mikami, S. Urata, N. Ando, Power generation of thermoelectric oxide modules, in: Proceedings of 24th International Conference on Thermoelectrics, Clemson, USA, 2005, pp. 295–302.
[11] J. Posthill, A. Reddy, E. Siivola, G. Krueger, M. Mantini, P. Thomas, R. Venkatasubramanian, Portable power sources using combustion of butane and thermoelectrics, in: Proceedings of 24th International Conference on Thermoelectrics, Clemson, USA, 2005, pp. 520–523.
[12] K. Yoshida, S. Tanaka, S. Tomonari, D. Satoh, M. Esashi, High-energy density miniature thermoelectric generator using catalytic combustion, IEEE/ASME. J. Microelectromech. Syst. 15 (2006) 195–203.
[13] US patent application publication 2006027258(A1).
[14] J.A. Federici, D.G. Norton, T. Bruggemanna, K.W. Voit, E.D. Wetzel, D.G. Vlachos, Catalytic microcombustors with integrated thermoelectric elements for portable power production, J. Power. Sources 161 (2006) 1469–1478.
[15] A.M. Karim, J.A. Federici, D.G. Vlachos, Portable power production from methanol in an integrated thermoeletric/microreactor system, J. Power. Sources 179 (2008) 113–120.
[16] R. Echigo, K. Hanamura, H. Yoshida, M. Koda, K. Tawata, Sophisticated thermoelectric conversion devices of porous materials by super-adiabatic combustion of reciprocating flow and advanced power generation system, in: Proceedings of 11th International Conference on Thermoelectrics, Arlington, USA, 1992, pp. 45–50.
[17] US patent 6613972.
[18] F. Katsuki, T. Tomida, H. Nakatani, M. Katoh, A. Takata, Development of a thermoelectric power generation system using reciprocating flow combustion in a porous FeSi2 element, Rev. Sci. Instrum. 72 (2001) 3996–3999.
[19] C.W. Park, M. Kaviany, Combustion-thermoelectric tube, J. Heat. Transfer ASME. 122 (2000) 721–729.
[20] T. Esarte, M. Gao, D.M. Rowe, Modelling heat exchangers for thermoelectric generators, J. Power. Sources 93 (2001) 72–76.
[21] F.J. Weinberg, D.M. Rowe, M. Gao, P.D. Ronney, On thermoelectric power conversion from heat recirculating combustion systems, Proc. Combust. Inst. 29 (2002) 941–947.
[22] L.E. Bell, Alternate thermoelectric thermodynamic cycles with improved power generation efficiencies, in: Proceedings of 22nd International Conference on Thermoelectrics, Hérault, France, 2003, pp. 558–562.
[23] T. Kyono, R. Suzuki, K. Ono, Conversion of unused heat energy to electricity by means of thermoelectric generation in condenser, IEEE. Trans. Energ. Convers. 18 (2003) 330–334.
[24] R. Suzuki, Mathematic simulation on power generation by roll cake type of thermoelectric double cylinders, J. Power. Sources 133 (2004) 277–285.
[25] D.T. Crane, G.S. Jackson, Optimization of cross flow heat exchangers for thermoelectric waste heat recovery, Energ. Convers. Manag. 45 (2004) 1565–1582.
[26] M. Gao, D.M. Rowe, Conversion efficiency of thermoelectric combustion systems, IEEE. Trans. Energ. Convers. 22 (2007) 528–534.
[27] J. Yu, H. Zhao, A numerical model for thermoelectric generator with the parallel-plate heat exchanger, J. Power. Sources. 172 (2007) 428–434.
[28] T.J. Hendricks, Thermal system interactions in optimizing advanced thermoelectric energy recovery systems, J. Energ. Resource. ASME. 129 (2007) 223–231.
[29] R.B. Peterson, The maximum power operating point for a combustion-driven thermoelectric converter with heat recirculation, J. Eng. Gas. Turbines. Power. ASME. 129 (2007) 1106–1112.
[30] S.A. Omer, D.G. InTeld, Design and thermal analysis of a two stage solar concentrator for combined heat and thermoelectric power generation, Energ. Convers. Manag. 41 (2000) 737–756.
[31] B. Zhu, H.J. Schock, T. Hogan, T.I-P. Shih, A numerical study of convective and radiative heat transfer between parallel plates connected by an array of rods, in: Proceedings of 44th AIAA Aerospace Sciences Meeting and Exhibit, Reno, Nevada, 2006, p. 0574.
[32] C.H. Kuo, P.D. Ronney, Numerical modeling of non-adiabatic heat-recirculating combustors, Proc. Combust. Inst. 31 (2007) 3277–3284.
[33] Y. Yang, X. Wei, J. Liu, Suitability of a thermoelectric power generator for implantable medical electronic devices, J. Phys. D: Appl. Phys. 40 (2007) 5790–5800.
[34] J.A. Federici, D.G. Vlachos, A computational fluid dynamics study of propane/air microflame stability in a heat recirculation reactor, Combust. Flame. 153 (2008) 258–269.
[35] N. Sloth, H. Thorkelsson, Stoker Simulation, Project Report 10th semester (Master thesis), Institute of Energy Technology, Aalborg University, 2007.
[36] D. Astrain, J.G. Vian, A. Martinez, A. Rodriguez, Study of the influence of the thermal resistance in a thermoelectric generation system, in: Proceedings of 6th European Conference on Thermoelectrics, Paris, France, P1-18-1-4, 2008.
[37] E. Elena, D.C. Looman, Finite elements for thermoelectric device analysis in ANSYS, in: Proceedings of 24th International Conference on Thermoelectrics, Clemson, USA, 2005, pp. 200–203.
[38] L. Helmers, E. Müller, J. Schilz, W.A. Kaysser, Graded and stacked thermoelectric generators-numerical description and maximisation of output power, Mat. Sci. Eng. B. 56 (1998) 60–68.
[39] A.E. Kaliazin, V.L. Kuznetsov, D.M. Rowe, Rigorous calculations related to functionally graded and segmented thermoelements, in: Proceedings of 20th International Conference on Thermoelectrics, Beijing, China, 2001, pp. 286–292.
[40] T. Hogan, T. Shih, Modeling and characterization of power generation modules based on bulk materials, Thermoelectrics Handbook: Macro to Nano, Ed. D M Rowe, Taylor & Francis: London, 2006, pp. 12.1–12.23.
[41] G. Danko, Functional or operator representation of numerical heat and mass transport models, J. Heat. Transf. ASME. 128 (2006) 162–175.
[42] J.S. Herring, J.E. O'Brien, C.M. Stoots, G.L. Hawkes, J.J. Hartvigsen, M. Shahnam, Progress in high-temperature electrolysis for hydrogen production using planar SOFC technology, Int. J. Hydro. Energ. 32 (2007) 440–450.
[43] M. Chen, L.A. Rosendahl, T.J. Condra, J.K. Pedersen, Numerical modeling of thermoelectric generators with varying material properties in a circuit simulator, IEEE. Trans. Energ. Convers. 24 (2009) 112–124.
[44] C.A. Domenicali, Stationary temperature distribution in an electrically heated conductor, J. App. Phys. 25 (1954).
[45] M. Chen, S.J. Andreasen, L.A. Rosendahl, S.K. Kær, T.J. Condra, System modeling and validation of a thermoelectric fluidic power source-proton exchange membrane fuel cell and thermoelectric generators (PEMFC-TEG), J. Electron. Mater. 39 (2010) 1593–1600.